THE UNIVERSITY of EDINBURGH

Edinburgh Research Explorer

# The Electrical Structure of the Central Main Ethiopian Rift as imaged by Magnetotellurics - Implications for Magma Storage and Pathways

**Citation for published version:**
Hübert, J, Whaler, K & Fisseha, S 2018, 'The Electrical Structure of the Central Main Ethiopian Rift as imaged by Magnetotellurics - Implications for Magma Storage and Pathways' Journal of Geophysical Research: Solid Earth. DOI: 10.1029/2017JB015160

**Digital Object Identifier (DOI):**
10.1029/2017JB015160

**Link:**
Link to publication record in Edinburgh Research Explorer

**Document Version:**
Publisher's PDF, also known as Version of record

**Published In:**
Journal of Geophysical Research: Solid Earth

**Publisher Rights Statement:**
©2018. American Geophysical Union. All Rights Reserved.

**General rights**
Copyright for the publications made accessible via the Edinburgh Research Explorer is retained by the author(s) and / or other copyright owners and it is a condition of accessing these publications that users recognise and abide by the legal requirements associated with these rights.

**Take down policy**
The University of Edinburgh has made every reasonable effort to ensure that Edinburgh Research Explorer content complies with UK legislation. If you believe that the public display of this file breaches copyright please contact openaccess@ed.ac.uk providing details, and we will remove access to the work immediately and investigate your claim.

OPEN ACCESS

Download date: 05. Apr. 2019

Journal of Geophysical Research: Solid Earth

RESEARCH ARTICLE
10.1029/2017JB015160

**Key Points:**
- We imaged the electrical structure of the CMER with magnetotellurics
- A mid-crustal cooled intrusive body is imaged as a resistor under Aluto volcano
- A highly conductive zone is found under the Silti Debre Zeyit Fault zone close to Butajira volcanic field

**Supporting Information:**
- Supporting Information S1

**Correspondence to:**
J. Hübert,
Juliane.huebert@ed.ac.uk

**Citation:**
Hübert, J., Whaler, K., & Fisseha, S. (2018). The electrical structure of the Central Main Ethiopian Rift as imaged by magnetotellurics: Implications for magma storage and pathways. *Journal of Geophysical Research: Solid Earth, 123*. https://doi.org/10.1029/2017JB015160

Received 27 OCT 2017
Accepted 2 JUN 2018
Accepted article online 9 JUN 2018

©2018. American Geophysical Union. All Rights Reserved.

# The Electrical Structure of the Central Main Ethiopian Rift as Imaged by Magnetotellurics: Implications for Magma Storage and Pathways

**Juliane Hübert**[1], **Kathy Whaler**[1], **and Shimeles Fisseha**[2]

[1]School of Geosciences, University of Edinburgh, Edinburgh, UK, [2]Institute of Geophysics, Space Science and Astronomy, Addis Ababa University, Addis Ababa, Ethiopia

**Abstract** The Main Ethiopian Rift is part of the East African Rift with its unique geological setting as an active continental breakup zone. The Main Ethiopian Rift includes a number of understudied active volcanoes with potentially high risks for this densely populated part of Ethiopia. Using newly recorded (2016) magnetotelluric data along a 110 km long transect crossing the whole rift, we present a regional 2-D model of electrical resistivity of the crust. The derived model endorses a previous study that drew the surprising conclusion that there was no highly conductive region associated with a magma chamber directly under the central rift volcano Aluto. This has implications for the estimation of the amount of magma present, its water content, and the storage conditions, as the volcano is actively deforming and results from seismicity and $CO_2$ degassing studies all indicate magma storage at about 5 km depth. Additionally, the existence of a strong conductor under the Silti Debre Zeyt Fault Zone approximately 40 km to the northwest of the rift center is confirmed. It is located with a slight offset to the Butajira volcanic field, which hosts a number of scoria cones at the boundary between the NW plateau and the rift. The magnetotelluric model reveals different electrical structures below the eastern and western rift shoulders. The western border is characterized by a sharp lateral contrast between the resistive plateau and the more conductive rift bottom, whereas the eastern flank shows a subhorizontal layered sequence of volcanic deposits and a smooth transition toward the shoulder.

## 1. Introduction

Deep electromagnetic sounding techniques such as magnetotellurics (MT) are formidable tools for imaging magmatic systems. The capacity of MT to characterize the subsurface electrical conductivity structure through measurements of the electromagnetic field at the surface contributes to the understanding of the plumbing system and magma storage in the crust and upper mantle, as electrical conductivity (or its inverse, electrical resistivity) is a rock parameter very sensitive to the presence of fluids and melt in the rock matrix. MT can usefully be combined with other geophysical methods such as seismology or GPS and deformation studies that characterize the mechanical properties of the rocks. Several examples of MT studies have been reported that identify conductive anomalies associated with zones of accumulated magma below active volcanoes, both at depths between 3 and 6 km and deeper in the lower crust. A prominent example in a continental arc setting is the massive lower crustal Altiplano-Puna magma body in the central Andes (Comeau et al., 2015), which has been interpreted as the very hydrous source of multiple andesitic and dacitic lava flows in several volcanic centers. Recent MT studies in areas with rift-related volcanism include Hengill, Iceland (Árnason et al., 2010; Rosenkjaer et al., 2015) where a good electrical conductor at 4.5 km below sea level was detected; Eyjafjallajökull, Iceland (Miensopust et al., 2014; Sigmundsson et al., 2010) with a highly conductive feature at depth and the Taupo Volcanic Zone in New Zealand (Bertrand et al., 2013, 2015; Heise et al., 2010) where both the Rohaki geothermal field and Ohaaki volcano are associated with good conductors at depth.

MT studies in the East African Rift and Afar in Ethiopia have a tradition as part of multidisciplinary investigations of the volcanism related to rifting processes. Previous surveys have highlighted the capability of MT to quantify the amount of magma present in the subsurface. Desissa et al. (2013) and Johnson et al. (2015) estimated magma volumes below the Manda-Hararo magmatic segment in Afar based on the observation of very high conductivities using models that link electrical conductivity to melt fractions. Further south in the Main Ethiopian Rift, Whaler and Hautot (2006) found that the subsurface was significantly less conductive than

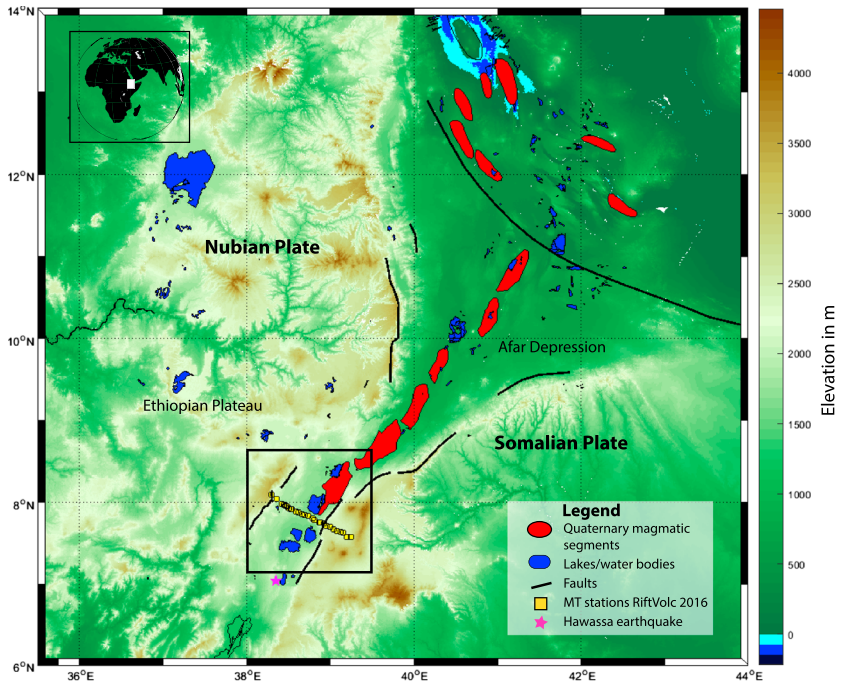


**Figure 1.** Topographic map of the Main Ethiopian Rift, part of the East African Rift (elevation data from the SRTM3 shuttle mission) with the location of magmatic segments (red shapes) after Ebinger and Casey (2001); border faults from Agostini et al. (2011; black lines); the Hawassa earthquake from January 2016 according to Wilks, Ayele, et al. (2017; magenta star) and magnetotelluric (MT) stations from the RiftVolc 2016 experiment (yellow squares).

in Afar but that there were still conductive features located below the rift axis as well as near the rift flanks. Samrock et al. (2015) investigated the central rift volcano Aluto that surprisingly did not exhibit a mid-crustal conductive feature, although their study indicated a conductor beneath one of the rift flanks. Selway (2015) investigated the electrical conductivity of the East African Rift and the Tanzanian Craton and in their model also found a conductive crustal body beneath Mount Kilimajaro. MT has also been used to investigate high enthalpy geothermal prospects within the region (e.g., Didana et al., 2015; Mwarikani, 2015; Wameyo, 2005).

In the following sections we present the analysis and interpretation of newly collected MT data along a cross-rift profile traversing Aluto volcano. A 2-D inversion model images the electrical resistivity structure of upper and middle crust of the Central Main Ethiopian Rift (CMER).

## 2. The Study Area in the Ethiopian Rift

The NE-SW trending Main Ethiopian Rift (MER, Figure 1) constitutes the youngest leg of the mid-ocean ridges and rift meeting at the Afar triple junction and is the southern continuation of this active continental breakup zone (Corti, 2009; Furman et al., 2006). The rifting process is characterized by multiple modifications of the crust. Weakening is caused by heating via dike intrusions (Daniels et al., 2014), whereas cooled gabbroic intrusions can increase crustal strength (Beutel et al., 2010). In the MER, recent volcanism is concentrated in the rift center, whereas some mechanical stress is released on the border faults of the rift shoulders. Strain and magmatism are segmented along the rift axis (Ebinger & Casey, 2001), and active volcanoes are positioned above Quaternary magmatic segments close to the axis (Rooney, 2010). The extension rate of about 6 mm/year in the CMER (Kogan et al., 2012) is accompanied by a moderate number of smaller earthquakes ($M_L < 3$, e.g., Wilks, Kendall, et al., 2017), but occasionally larger events on the border faults are recorded. Recently (on 26 January 2016), a 4.5 magnitude earthquake was located and widely felt near Hawassa (Wilks, Ayele, et al., 2017; see Figure 2).

Our study area is in the lakes region of the CMER (see Figure 2). Here, the Moho depth is estimated at between 36 and 42 km below the rift and the eastern shoulder but thought to be thinner under the SW shoulder and the Debre Zeyt (Bishoftu) volcanic field to the NW (Stuart et al., 2006). The CMER hosts several active volcanoes with caldera edifices (Peccerillo et al., 2003) and a large number of monogenetic vents

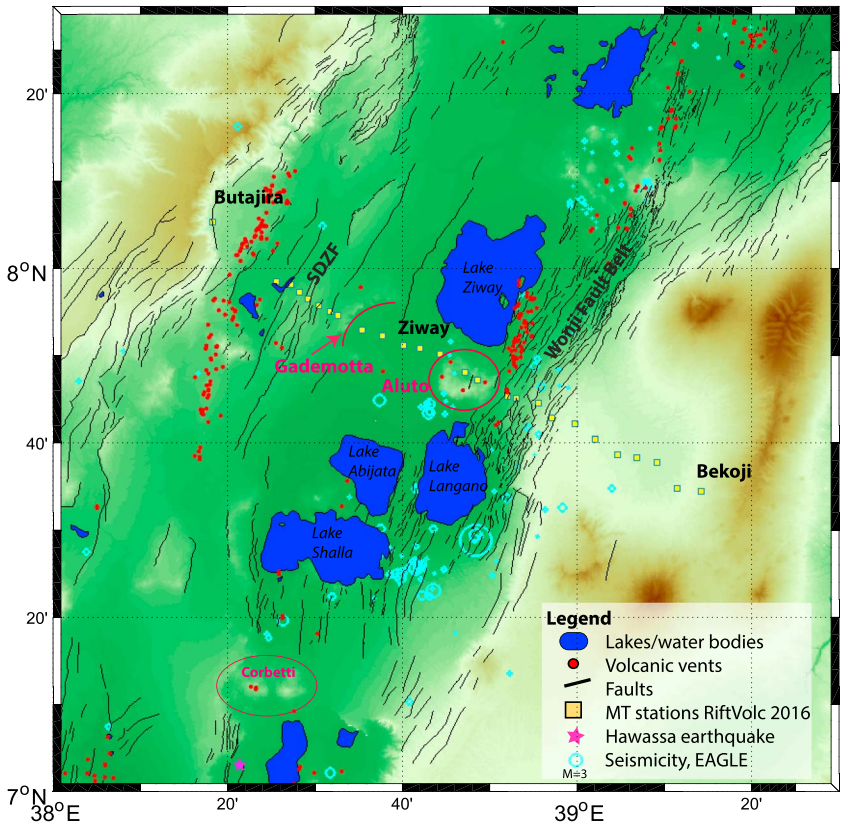


**Figure 2.** Map of the study area (black square in Figure 1) with the location of Aluto and Corbetti volcanoes as well as the Gademotta caldera (red circles/arcs), earthquakes recorded in the EAGLE experiment (cyan circles) after Keir et al. (2006), and volcanic vents (red dots) from Mazzarini and Isola (2010). Faults on the eastern side of Aluto belong to the Wonji Fault Belt, to the west to the Silti Debre Zeyt Fault Zone (SDZF).

(Mazzarini et al., 2016; Rooney, 2010), and sources of hydrothermal activity. Pulse-like surface deformation events on a number of volcanoes located on the central rift axis have been reported through the analysis of satellite imagery (interferometric synthetic aperture radar, InSAR; Biggs et al., 2011) and give rise to concern about potential geohazards associated with volcanic activity. The silicic peralkaline volcano Aluto has been the target of a number of geological, geochemical, and geophysical studies undertaken in recent years (Fontijn et al., 2018; Gleeson et al., 2017; Hutchison et al., 2015; Hutchison, Biggs, et al., 2016; Hutchison, Mather, et al., 2016; Saibi et al., 2012; Teklemariam et al., 1996; Wilks, Kendall, et al., 2017). It is the site for a hydrothermal power plant with three test drillings awaiting integration into the local power grid. Its 14 km wide edifice with an elliptically east-west elongate caldera rises approximately 700 m above the rift floor. Aluto has undergone several effusive eruption events and is now at a post-caldera stage with eruption products of highly felsic composition such as rhyolitic lava flows and pumice cones. There is evidence for pyroclastic density currents with faults dissecting the volcanic complex as seen from exploration wells. Magma composition at depth is thought to be of pantellerite and comendite composition (Fontijn et al., 2018; Gleeson et al., 2017; Hutchison, Mather, et al., 2016). Periods of deformation of Aluto have been reported from InSAR and GPS signal analysis over the past 13 years with rapid uplift events with displacement of about 10–15 cm in 2004 and subsequent slower subsidence followed by another 10 cm uplift at the end of 2008 (Biggs et al., 2011). This deformation was modeled and attributed partly to a shallow source, representing processes in the hydrothermal system at 1- to 2 km depth and partly to a deeper source (5 km), which has been interpreted as the location of stored magma (Hutchison, Biggs, et al., 2016). The analysis of increased $CO_2$ degassing along the caldera faults (Hutchison et al., 2015) also indicates a deeper source of the magmatic processes. Seismic studies (Wilks, Kendall, et al., 2017) located increased activity at the edge of the proposed magma storage region. Mickus et al. (2007) presented band-passed-filtered gravity data that image Bouguer gravity maxima associated with the magmatic segments located under the volcanic centers of Aluto and Corbetti

to the SW (Figure 2). A 2.5-D model considering constraints from seismic velocity models contained a high-density body approximately 3,000 kg/m$^3$ in the lower crust (7–17 km) below Aluto, which was interpreted as a large, cooled mafic intrusion.

Samrock et al. (2015) performed a MT survey to investigate the electrical conductivity structure under Aluto. They collected high-quality MT data in an array on and around the volcanic edifice and identified a shallow zone of higher conductivity as the clay cap over the hydrothermal system. There was no evidence in their electrical conductivity model for a deeper conductive anomaly that could represent interconnected magma storage, but the limited aperture of their station array made the detection of deeper structures a challenge. Instead, they postulated the existence of a regional very conductive feature 40 km to the west of Aluto close to the Silti Debre Zeyt Fault Zone (SDZF) from forward modeling of the data, which could not be explained by any parts of the model below Aluto. The SDZF constitutes the western part of the CMER and hosts a substantial amount of Quaternary mafic volcanism in the form of monogenetic vents (Rooney et al., 2005, 2007; Woldegabriel et al., 1990) in a narrow band surrounded by a wider zone of seismicity (Keir et al., 2015).

Aluto's caldera is dissected by faults belonging to the Wonji Fault belt (WFB), which lies between the rift axis and the eastern shoulder. It comprises a dense and complex network of short and closely spaced faults with relatively small throw (< 100 m), steep scarps, and dense horst and graben structures with subvertical dips (< 65°) and roughly (axis 12°N) east-west extension (Mohr, 1967). It has no associated increased $CO_2$ degassing signature (Hunt et al., 2017). Further to the north, it is associated with Quaternary volcanism and the accommodation of stress through brittle deformation. This signifies a shift at this stage of the rifting away from deformation at the larger border faults (Corti, 2009). There is evidence for off-axis magmatism in the presence of monogenetic vents (see Figure 2).

## 3. The Electrical Conductivity of Peralkaline Melts

The bulk electrical conductivity of a rock-melt system is dominated by the conductivity of the melt phase. The melt conductivity is in turn dependent on composition, temperature, pressure, and fluid content (e.g., Roberts & Tyburczy, 1999) and can be investigated in laboratory settings. Laboratory experiments and petrological modeling of the electrical conductivity of melt and melt-rock phases are at the center of ongoing research (Pommier, 2014). Gaillard (2004) investigated the conductivity of hydrous and dry silicic melts and found that the main contributor to the electrical conduction mechanism is the mobility of sodium ions, which are abundant in alkaline magmas (see also Pommier et al., 2010). Additionally, increased water content was associated with higher conductivities through an enhancement of the ions' mobility. The latest contribution to the study of electrical properties of peralkaline melts is that of Guo et al. (2016), who concluded that the water content of the melt component is the crucial factor for the electrical resistivity. They observed slightly higher (three quarters of a magnitude) resistivities than Pommier and Le-Trong (2011) for silicic melts and postulated an empirical relationship between melt resistivity, water content, temperature, and pressure. Using two-phase mixing models such as those based on the Hashin-Shtrikman bounds (Hashin & Shtrikman, 1962) that describe the geometry of the melt in the rock matrix allows for estimates of melt fraction from observed bulk resistivities. These range from formulae for well-connected melt, giving the minimum fraction for a given bulk resistivity, to those for unconnected melt pockets, when higher fractions are inferred.

## 4. The Magnetotelluric Method

MT probes the subsurface electrical conductivity (or its inverse, electrical resistivity) through the measurement of the naturally occurring electrical and magnetic fields on the Earth's surface that are induced by a changing external magnetic field. Introduced by Cagniard (1953) and Tikhonov (1950), it is now widely used for the characterization and exploration of the subsurface from shallow depths down to the upper mantle. The period (or its inverse, the frequency) of the electromagnetic signals, along with the electrical conductivity of the subsurface, determines how far the signal propagates, and hence indicates an appropriate station separation. The skin depth, defined as the depth in a uniform conductivity medium at which the amplitude is attenuated to $1/e$ of its surface value, is a useful indicator of the penetration depth. Longer periods yield deeper investigations but require longer recording times. As a passive method it is susceptible to cultural noise caused by artificial electrical sources, vibrations, etc., but this can be somewhat mitigated by robust data processing techniques. The horizontal electric and the vertical magnetic field components ($E_x$, $E_y$, and $H_z$) are related through transfer functions to the horizontal magnetic field components ($H_x$ and $H_y$).

Estimated as a function of period, the transfer function components embed the information about the subsurface resistivity distribution and hence are referred to as the data. The MT transfer function relating electric field components ($E$) to the magnetic field ($H$) is called the impedance tensor ($Z$), defined by $E = ZH$. The complex components of $Z$ can be displayed as frequency-dependent apparent resistivity ($\rho_a$) and phase ($\phi$). Mathematical analysis of the tensor can be used to infer the complexity or dimensionality of the underlying electrical conductivity structure. For example, the diagonal impedance elements vanish in a one-dimensional subsurface, and also in a two-dimensional subsurface so long as the coordinate system is aligned with geoelectrical strike, defining the direction of current flow. Hence, performing a strike analysis by rotating the coordinate system to find the direction minimizing the diagonal impedance tensor components, and ascertaining whether they are vanishingly small, is often undertaken. Analysis of the phase components of $Z$, known as the phase tensor, also provides dimensionality information, with the advantage that the results are unaffected by galvanic (i.e., non-inductive) effects in the near-surface (Caldwell et al., 2004). Galvanic effects appear in 2-D apparent resistivity data as a constant vertical offset of apparent resistivity plotted as a function of period; hence, galvanic distortion is often referred to as static shift. The inducing magnetic field is assumed to be vertical, and accordingly, a nonzero induced vertical magnetic field indicates lateral variations in electrical conductivity. The transfer function between the vertical and the horizontal components of the magnetic field is called the tipper or vertical magnetic transfer function. Inversion algorithms are used to reconstruct electrical resistivity models that explain the transfer function data and allow for geological interpretations.

## 5. New MT Data Along a Cross-Rift Transect

In January and February 2016 new broadband MT (BMT) data at 29 sites and long period MT (LMT) data at three sites were collected along a 110 km long transect (see Figure 2) starting near Butajira on the western edge of the rift, crossing Aluto, and passing the WFB and the eastern border faults into the highlands near Bekoji. Spacing between the sites varied between 2.5 km in the SDZF (because of the suspected higher electrical conductivity there) and 5 km elsewhere. BMT data were collected during 24 hr installations, but had mixed quality due to the dense population of the area leading to relatively high cultural noise levels. The LMT sites recorded for 2–3 weeks, two of them producing usable transfer functions. Robust time series processing of the BMT data to calculate transfer functions was performed with the algorithm of Egbert (1997); for the LMT recordings we used the processing method of Smirnov (2003). Both impedance and tipper transfer functions were estimated in a broad frequency range, from a maximum of 300 to 0.001 Hz at most sites; transfer functions down to 0.0001 Hz were achieved only for site LMT2 (Figures 3 and 4). Data collected in the center of the profile close to the Trans-African Highway and the greenhouse industrial complex were generally noisier than in the more remote areas of the flanks of the rift. The amplitude and variations in the vertical component of the magnetic field ($H_z$) were very small except close to Aluto and therefore also more influenced by noise. Tipper data were consequently neglected in the following analysis, except to note that their small values support a 2-D interpretation of the data.

On the edifice of Aluto, we installed four BMT stations in locations previously occupied by Samrock et al. (2015). Industrial activity in the power plant and electrical noise levels seemed to have increased since the previous field campaign in 2012 as the direct comparison of the data collected at these locations showed. Nevertheless, the derived impedance transfer functions were very similar. No systematic differences were observed that could be associated with subsurface changes in the electrical structure in connection with the deformation events detected by both GPS and InSAR (Hutchison, Biggs, et al., 2016).

The phase tensor (Caldwell et al., 2004), calculated from the impedance, is unaffected by static shift and can be visualized through its skew (beta) angles and ellipses whose values, aspect ratio, and axes directions indicate data dimensionality and geoelectric strike. Our data have very small beta values and rounded ellipses (Figure 3). This and strike and dimensionality analysis reveal that the data are surprisingly low dimensional for the shorter periods (up to 1 s), except directly below the volcano and for the longer periods in the western part of the profile. We performed a strike analysis after Zhang et al. (1987) but no dominant geoelectrical strike angle was found (see supporting information Figure S1). The low degrees of dimensionality, supported by the small tipper values, therefore allow for a two-dimensional (2-D) interpretation of the data. In the absence of a well-defined geoelectrical strike direction, we chose an angle of 28°N, consistent with the trend of the rift. Previous MT studies in Ethiopia have found dominantly rift-parallel geoelectrical strike directions (e.g., Desissa et al., 2013; Whaler & Hautot, 2006). The positions of the stations were accordingly projected onto a profile line perpendicular to the strike. The impedance tensor elements can be rotated into the coordinates

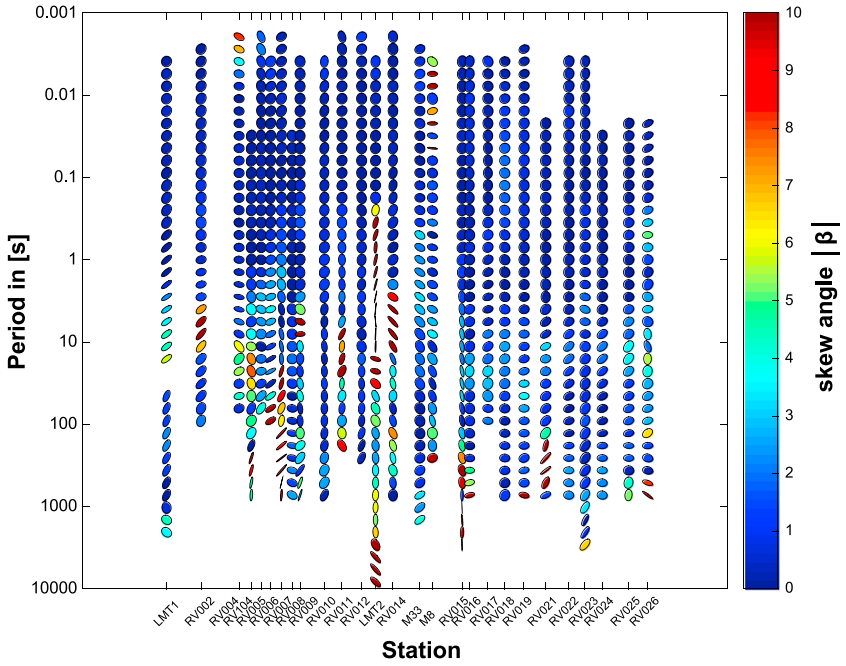


**Figure 3.** Phase tensor from MT data along the profile for all recorded periods (after Caldwell et al., 2004); the fill colors are the skew angles $\beta$. Most stations and period ranges show low skew values ($|\beta| < 4°$), which justifies a 2-D inversion approach (e.g., Booker, 2014; Pous et al., 2011).

defined by the strike direction to define the transverse electric (TE) and transverse magnetic (TM) modes of induction, describing currents flowing along and perpendicular to strike, respectively. For low dimensionality data, such as in this study, the determinant average of the impedance tensor elements (DET) is also a useful quantity, because it is rotationally invariant, that is, not dependent on the geoelectric strike direction.

Our model area was discretised into rectangular cells of constant resistivity, using standard guidelines for cell sizes and the area modeled. For the 2-D inversion of the impedance data we used the package EMILIA by Kalscheuer et al. (2008), which offers a variety of regularization schemes for a finite difference approach including modified rebocc (after Siripunvaraporn & Egbert, 2000). We inverted the apparent resistivity and phase of the determinant (DET) mode and jointly the TE and TM modes starting from a homogeneous half space of 100 Ωm. Different half space resistivities for the starting model were tested but found not to be of significance to the final model and to the minimum root-mean-square (RMS) achieved. In addition to the measurement random errors, we tested different error floors (10%, 30%, and 90%) to account for static shift on the apparent resistivity curves for the DET and the TE mode. Static shift on the TM or DET mode is compensated for by a fine model discretization between adjacent stations along the profile, where the inversion is free to introduce small near-surface heterogeneities (Pedersen & Engels, 2005). However, using the increased error floors did not result in very different model features and caused only minimal changes to the final RMS. The preferred model was obtained by inversion of the DET mode with a 10% error floor on apparent resistivity and 2.5° on the phase data. Models derived from TE, TM, and joint TE TM mode inversions (see supporting information Figures S3–S5) contain very similar features, but data fit was best in the determinant mode model.

In the inversion, we started with a model space approach with occam-style (smoothness-constrained) regularization that produced a minimum RMS of 1.18 after three iteration but would not converge further, instead producing oscillating RMS in any further iterations. We then restarted the inversion using the model with the lowest RMS as the starting model for a Levenberg-Marquardt inversion (Kalscheuer et al., 2010) that stabilized the convergence and brought the RMS further down to 0.99 (see supporting information Figure S2), signifying that the derived 2-D model is able to explain the observed data within the specified error bars (see Figure 4).

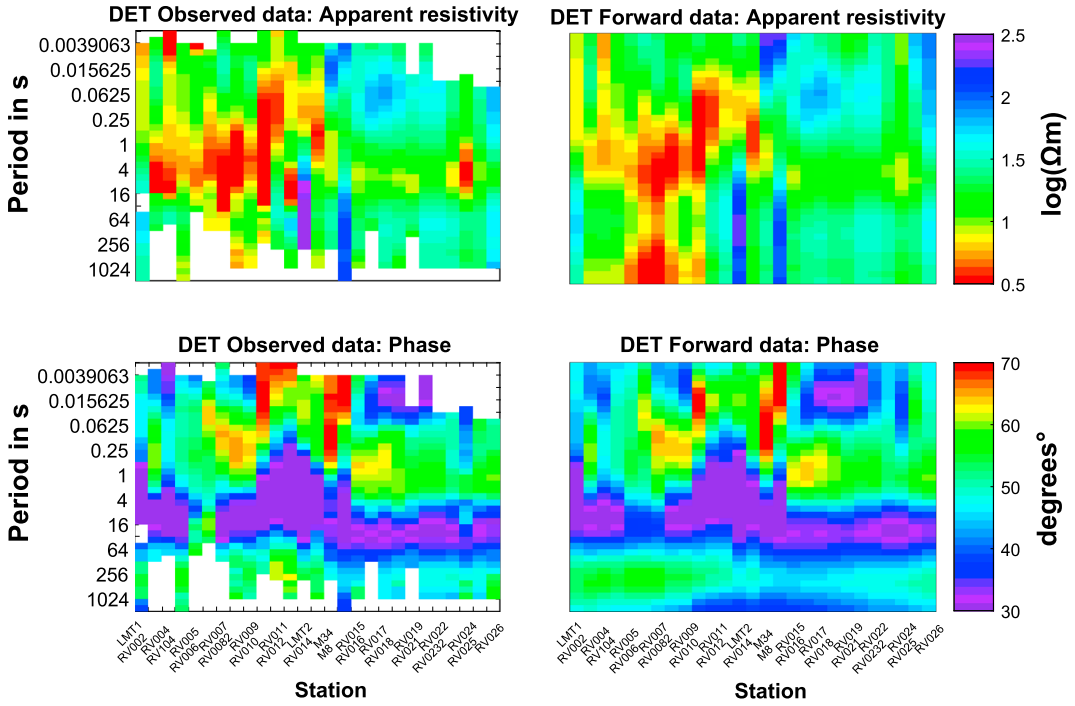


**Figure 4.** MT determinant data shown in pseudosection, top panel: Apparent resistivity; lower panel: Phase. Left: Observed apparent resistivity and phase; right: Calculated data for the preferred inversion model in Figure 5.

## 6. The Electrical Resistivity Model Along the Transect

The preferred 2-D model along the profile to a depth of 30 km is depicted in Figure 5 and reveals an asymmetric electrical structure across the CMER. At the western end of the profile, there is a strong lateral change in electrical resistivity from the more resistive regime of the rift shoulders toward the bottom of the rift valley. Following the profile to the east, the model shows a very prominent subvertical near-surface conductor (less than a kilometer wide) close to the SDZF zone near Butajira that is connected to a deeper and laterally more extensive zone of enhanced electrical conductivity (resistivity below 1 Ωm). The lower boundary of this deeper conductor is not resolved and, at depth, it is smeared laterally by the regularization scheme. Two distinct resistive bodies (< 500 Ω m) are located in the center of the profile below Aluto and the extinct Gademotta caldera west of Ziway (Figure 2), starting at 1 km depth and extending to below 15 km. East of Aluto in the WFB and continuing beyond the border faults into the highlands near Bekoji, there is a sequence of thin subhorizontal layers of alternating lower and higher resistivities up to 5 km depth. Below, a resistive layer extends to about 15 km depth. Under Aluto, the subsurface is resistive at depths < 3 km, which confirms the results from the much higher-resolution 3-D model from Samrock et al. (2015), but which was based on a smaller array aperture - and hence limited depth resolution - of MT stations around the volcano edifice. With the frequency content of our data and the profile length in this study, we would have identified a deeper conductive anomaly under or around Aluto that might be expected from significant amounts of magma or partial melt, known to be present from geodesy, seismology, and degassing studies, had it existed.

## 7. Model Assessment and Robustness of Features

In order to investigate the robustness of the deeper conducting feature below the SDZF (bearing in mind that the data penetration depth will be restricted there), a forward modeling sensitivity test was performed. We modified the preferred model (Figure 5) by removing the deep conductor and replacing it with material of 15 Ωm (typical of resistivities found elsewhere along the profile). Calculating the forward response, the overall RMS misfit of the modified model increased to 1.25. Comparing the forward responses (see supporting information Figures S3 and S4) of both the preferred and the modified inversion model shows that the greatest effect is seen in the apparent resistivity data above 64 s period. Additionally, there is a systematic mismatch in the phase values for both the stations directly above and further to the east of the conductor, which are

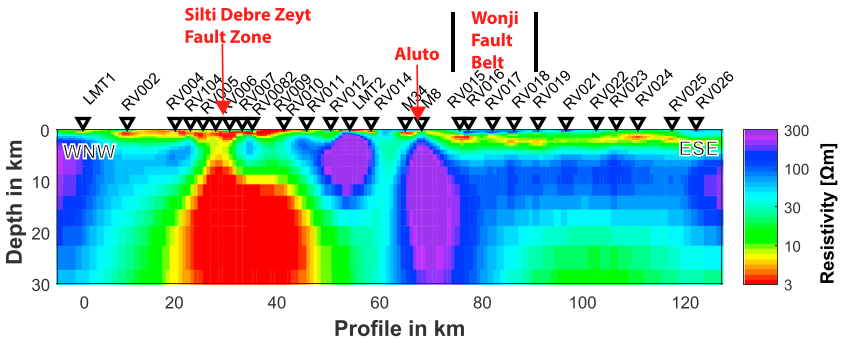


**Figure 5.** Preferred inversion model of electrical resistivity for the upper 30 km along the profile with station locations and position of major tectonic features.

better reproduced in the preferred inversion model. This confirms that the presence of a deeper conductor is required to explain data from the western-central section of the profile and is in accordance with the forward modeling of tipper data on Aluto by Samrock et al. (2015). We also tested the sensitivity of the MT data to a conductive feature representing a shallow magma chamber under Aluto and found that the presence of such a feature would easily be detected by the data collected above it (see supporting information Figure S3). The overall RMS of the model containing such a conductive anomaly is 1.86, and the mismatch in the apparent resistivity and phase curves of measured and calculated data is evident for periods < 1 s.

## 8. Discussion

### 8.1. Melt Storage Under Aluto

Recent studies of InSAR (Biggs et al., 2011), seismicity (Wilks, Kendall, et al., 2017), and GPS data studies on Aluto and the presence and nature of $CO_2$ degassing along the caldera faults (Hutchison et al., 2015) have all concluded that there is a source of magmatic activity at around 5 km depth. Surprisingly, no deeper conductive anomaly below Aluto is imaged by MT. Our field survey would have detected a magma chamber with well-connected partial melt: the length of the profile and the frequency content of the data (LMT2 close to Aluto has stable transfer functions at periods > 1,000 s) are more than sufficient to image this upper crustal feature. From the dimensionality analysis and very small tipper values, we conclude that there are no indicators for off-profile conductors in the data, so we consider the absence of a conductive anomaly at the proposed depth of the magma chamber as a robust feature in our model and not an MT resolution issue. This is in stark contrast to the situation elsewhere in the MER and Afar, where the presence of magma is associated with an electrically conducting subsurface (e.g., Didana et al., 2015; Johnson et al., 2015; Whaler & Hautot, 2006). This first order contradiction between our MT results and other geophysical and geochemical observations gives new insights into the storage of melt under an on-axis volcano in the CMER. Electrical resistivity of melts involves the interplay of composition, melt fraction, and water content. The composition of the eruptive products of Aluto are highly peralkaline (pantellerite and comendite, Fontijn et al., 2018), but this might differ from the current composition of melt present at depth. Peralkaline melts have increased electrical conductivity (compared to basaltic compositions) due to the presence of free sodium ions (Gaillard, 2004). However, the major contributor to electrical conductivity in these melts has been identified as the water content (Guo et al., 2016). We extrapolated Guo et al. (2016) results for the lower temperature and pressure regime of assumed magma storage at Aluto using their empirical relationship between electrical resistivity, water content, temperature, and pressure. Pre-eruptive magma conditions at Pantelleria, Italy—the type location for rhyolithic explosive volcanism—have been estimated through phase equilibrium studies by Di Carlo et al. (2010).

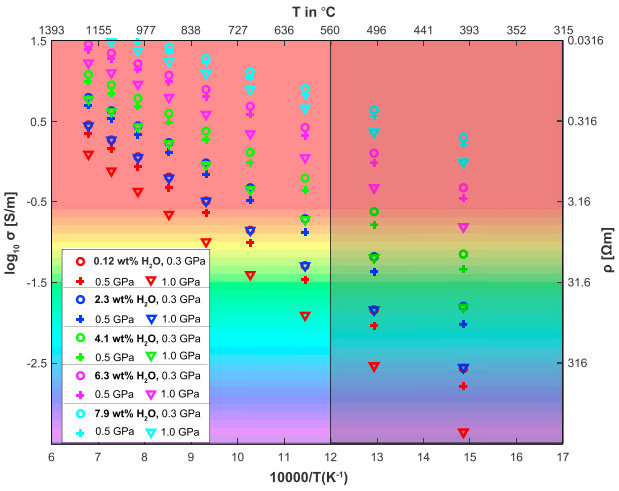


**Figure 6.** Computed electrical resistivity values for partial melt using the empirical relationship derived by Guo et al. (2016) for peralkaline melts. We extended the range for temperature (shaded part of the plot with $T < 560$ °C) by interpolating from the empirical relationship found by the authors: $\log \sigma = 2.983\text{-}0.0732w(3528 - 233.8w + (763 - 7.5w^2)p)/T$, with $\sigma$ the electrical conductivity in S/m, $T$ temperature in K, $w$ the $H_2O$ concentration in wt%, $p$ pressure in GPa. Their results illustrate that the electrical resistivity is very strongly influenced by the water content in the melt and can cause variations of several orders of magnitudes (values of 1 Ωm for 8 wt% $H_2O$, but > 300 Ωm for <1 wt% $H_2O$). Color scale of the background is the same as for the resistivity model in Figure 5.

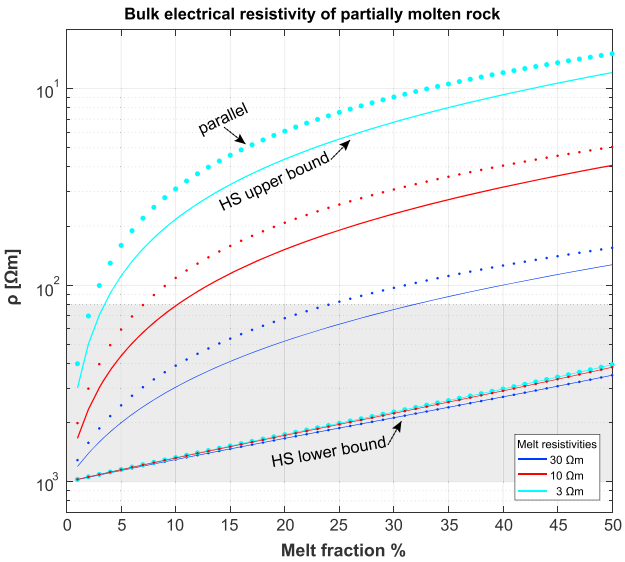


**Figure 7.** Bulk electrical resistivity of a two-phase system depending on the melt fraction for three different melt resistivities (33, 10, and 3 Ωm), and three different mixing modes: Parallel, Hashin-Shtrikman (HS) upper bounds, and HS lower bounds (Hashin & Shtrikman, 1962). The shaded area marks the resistivity range observed under Aluto in the preferred model.

For the most powerful post-caldera eruption they estimated that the magma containing 4 wt% $H_2O$ was stored at 4 km depth (100 MPa) and 680–720 °C. With similar water content (<4 wt%) for magma below Aluto, resistivities for silicic melts can be 3–10 Ωm (for temperatures around 700 °C; see Figure 6). This would result in bulk resistivities of > 300 Ωm for melt fractions below 10% using the Hashin-Shtrikman upper bound (Schmeling, 1986; see Figure 7) appropriate for a poorly connected melt such as the highly crystallized mush with potentially only small lenses of peralkaline melt inferred beneath Aluto (Gleeson et al., 2017).

Seismic activity at Aluto from 2012 to 2014 was studied with 11 broadband seismometers located on and closely around the volcano's edifice (Wilks, Kendall, et al., 2017). Most recorded events had $M_L \leq 3$ and are located in the shallow subsurface (i.e., in the uppermost 500 m). Between 500 m and 2 km depth, few earthquakes were recorded, but below that seismicity increases again. These deeper earthquakes coincide with the upper part of one of the resistive features in the electrical conductivity model and follow the lateral extension of this body (Figure 8).

The two large resistive features below Aluto and the Gademotta caldera (Figure 8) are interpreted as partially crystallized igneous bodies in the crust. Resistive bodies in the close vicinity of active volcanoes have been reported beneath Boset in the Northern Main Ethiopian Rift (EAGLE profile, Whaler & Hautot, 2006), and worldwide (Aizawa et al., 2014; Díaz et al., 2015). The electrical resistivity of gabbro at crustal pressure and temperature regimes has been estimated at 300–1,000 Ωm in laboratory experiments by Dai et al. (2015). At the Gademotta caldera, no recent volcanic activity has been reported (Woldegabriel et al., 1990); therefore, the presence of a cooled igneous body (which would have higher electrical resistivity) is reasonable. Mahatsente et al. (1999) reported a positive Bouguer anomaly in the CMER (see Figure 9), and Peccerillo et al. (2003), Cornwell et al. (2006), Mickus et al. (2007), Lewi et al. (2016), and others have interpreted such higher-density bodies as crystallized gabbroic crustal magmatic intrusions. The 3-D modeling of the gravity data by Mahatsente et al. (1999) included only one high-density body swelling up from the upper mantle directly below Aluto but did not fit a second positive anomaly in their data further to the west that could be associated with the resistive Gademotta caldera. Unfortunately, the sparser data sampling of the gravity measurements on the flanks of the rift does not match the density of the MT sites (see Figure 9), making a joint inversion of MT and gravity data that could provide constraints on both shape and depth extend of these bodies unfeasible. Time scales for the cooling of crustal magma bodies with equivalent volumes are estimated around 100 ka (Krumrei et al., 2006; McBirney, 1996), which is well within the time frame of the post-caldera stage of Aluto (Fontijn et al., 2018). Daly et al. (2008) found exceptionally low $V_p/V_s$ values beneath Aluto at 12 km depth consistent with the presence of cooled mafic intrusions,

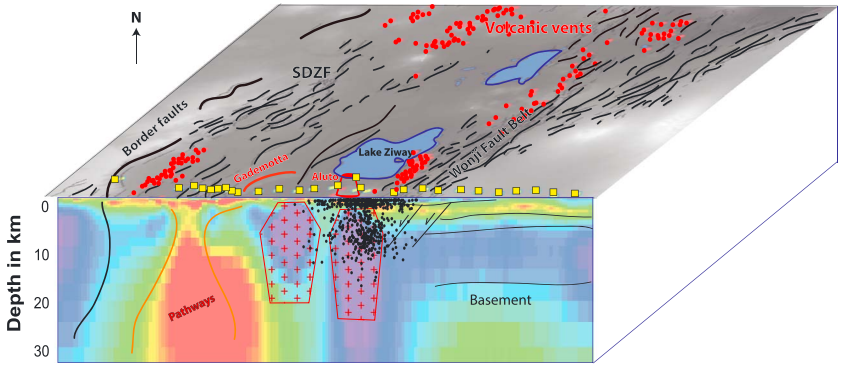


**Figure 8.** The Central Main Ethiopian Rift with the inferred position of crustal igneous bodies and magma pathways. Red dots: Volcanic vents; black lines: Fault lines; yellow squares: MT stations; small black circles: Seismic events from ARGOS experiment (Wilks, Kendall, et al., 2017). SDZF = Silti Debre Zeyt Fault Zone.

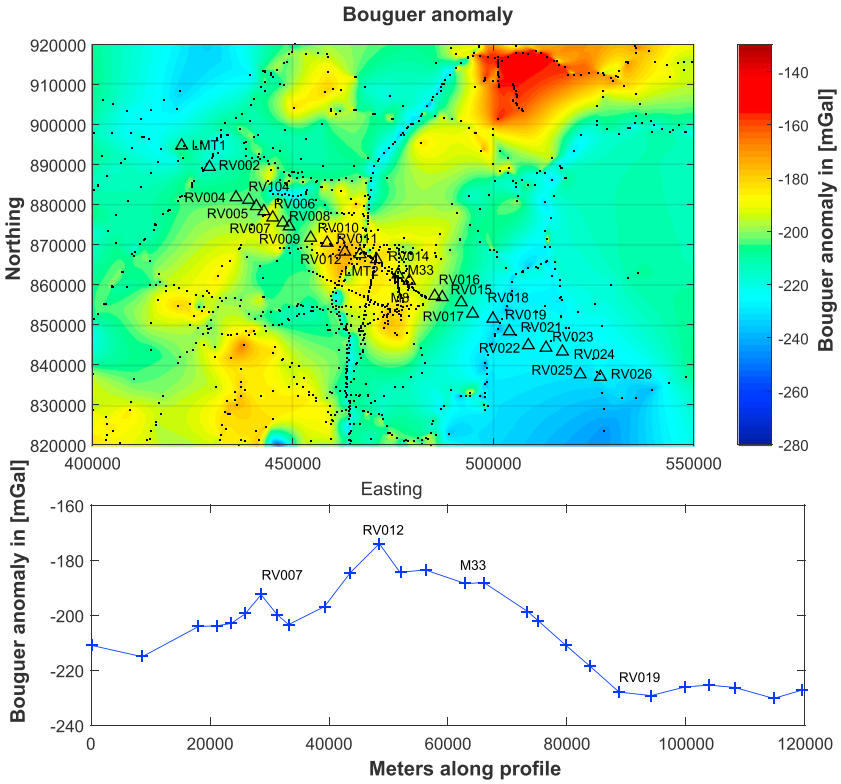


**Figure 9.** Bouguer anomaly data, reproduced from Mickus et al. (2007); upper panel: Map view with the location of MT stations (triangles) and gravity measurements (black dots). Interpolation used a Delauney triangulation. Lower panel: Extracted Bouguer anomaly at MT stations along profile. The long wavelength trend with a high over the rift center should be attributed to the upwelling of the asthenosphere under the rift, but the smaller positive anomalies (at stations RV012 and M33) can be explained by crustal high-density bodies.

and generally low ratios in the lower crust. In fact, their values are even smaller than those expected for cooled mafic intrusions, but they note that their values are lower than those obtained in other tomographic studies (e.g., Stuart et al., 2006).

### 8.2. The Conductor Under the SDZF Close to Butajira

Samrock et al. (2015) proposed the presence of a good conductor under the SZDF 40 km to the west of Aluto through forward modeling of tipper data on and around the volcano. Apart from a number of active faults, the SDZF is characterized by a large number of monogenetic vents connected to the failed Quaternary magmatic Butajira segment (Keir et al., 2015; Rooney, 2010; see Figure 8). The distribution of these scoria cones and the elongation of the volcanic fields in the MER have been analyzed by Mazzarini and Isola (2010), Mazzarini et al. (2013, 2016). They concluded that off-axis volcanic fields located closer to the rift margins have a high vent density but only moderate strain rates, whereas areas closer to the rift axis (e.g., the WFB) are characterized by higher rates of seismicity. The orientation of the volcanic fields is subparallel to the actual rift axis, showing rotation angles of about 15–20°, which is explained by preexisting crustal weaknesses and/or the geometry of the underlying magma reservoir. Our profile data and 2-D model cannot indicate the along-rift extent of this conductive feature.

Findings from ambient seismic noise studies (Kim et al., 2012) reveal mid-crustal low-velocity zones beneath the SDFZ. Stuart et al. (2006) find a high $V_p/V_s$ ratio (2.06) indicating the presence of crustal melt. Dugda et al. (2005) were unable to identify seismic phases needed to infer Poisson's ratio at site BUTA (Butajira); in Afar, the low amplitude of these phases was attributed to attenuation by abundant lower crustal melt (Ebinger et al., 2017). Consistent with geochemical analyses (Rooney et al., 2005, 2007) and the vent clustering (Mazzarini et al., 2013), magma ascent below the SDFZ is more complex with various depth levels of magma stalling, fractionation, and crystallization. Note that the limited depth resolution beneath the SDFZ conductor means we are unable to constrain reliably the depths or volumes of magma there.

### 8.3. The Wonji Fault Belt and the Eastern Edge of the Rift

On the eastern part of the transect, only subtle lateral changes in the electrical conductivity are observed below the WFB, which is both an area of increased seismicity and monogenetic vents (see Figure 2). There is no change in electrical resistivity associated with the border fault on the eastern shoulder of the rift, which is quite surprising as cross-rift seismic and MT profiles further north detected much sharper boundaries (Mackenzie et al., 2005; Whaler & Hautot, 2006). The electrical conductivity structure on the eastern flank of the CMER is mostly a layered sequence of resistive-conductive-resistive units, representing different volcanic products of various past eruptions. A more resistive (200 Ωm) layer in the very shallow subsurface (<200 m depth) just east of Aluto thins out and eventually disappears on the eastern end of the profile close to Bekoji. It is overlying a conductive feature with a thickness of about 2.5 km on top of older and less conductive units that extend to about 10 km depth. The upper boundary of the resistive layer is mostly flat with slight undulations.

### 8.4. Asymmetry of the Rift Shoulders

Compared to the EAGLE results 150 km along the rift to the north (Whaler & Hautot, 2006), the asymmetry of the rift is reversed: their MT profile has a sharp lateral boundary toward the Somalian plate and a more layered structure toward the northwestern flank. This type of along-strike asymmetry reversal has been reported in the Central African Rift by Bosworth (1992) who attributed these opposing dips/alternating detachments to pre-rift-existing weaknesses in the crust. On the surface this is reflected in the topography—on the EAGLE profile, the northern shoulder slopes down into the rift valley more gently than on the southern side where a couple of steep faults decent from the Somalian plateau. The situation is reversed for the presented profile, where the northwestern border close to Butajira is composed of a sharp climb onto the escarpment and a gentler ascent on the WFB side toward the southeast (see Figure 8). The presence of a highly conductive region (indicating well-connected magma and/or fluids present in the crust) under the southern SDZF but not under the WFB endorses Rooney et al. (2007) theory of a more complex magma storage system under the western part of the CMER compared to the east.

## 9. Conclusions

We have used newly collected broadband and long period MT data along a 110 km transect crossing the active post-caldera stage volcano Aluto to image the underlying electrical resistivity structure of the CMER. The dominant feature in the model is a subvertical conductor (< 10 Ωm resistivity) below the SDZF. Model assessment using forward modeling of perturbed resistivity distributions shows that MT data along most of the profile is sensitive to this conductor. Conductive anomalies with this amplitude are very likely to be associated with partial melt and/or fluids in dikes or faults and will aid in further investigation of the structural relationship to the Butajira volcanic field. Below Aluto, there is no conductive region at 5 km depth where magma storage is indicated by a number of other investigations including InSAR, seismology, and $CO_2$ degassing studies. This implies that the predominantly peralkaline melt is present in a highly crystallized mush or disconnected melt pockets. Relatively low water content (< 4 wt%) also leads to higher melt resistivities. The MT model includes two resistive bodies in the upper crust below Aluto and further to the west under the extinct Gademotta caldera. Including the observations and results from previous gravity studies, we suggest that the high resistivities are caused by large, cooled igneous bodies that have intruded the crust. Furthermore, the model images a sharp lateral resistivity contrast with higher resistivities outside the rift on the western flank below the steep escarpment close to the active boundary faults. The eastern part of the rift and the WFB are dissimilar by showing no lateral resistivity changes, which is in contrast to an MT model from the northern MER that showed a steep change on the eastern flank and more a horizontally layered structure to the west. These observations might be indicative of alternating detachments along the rift and an asymmetric stress accumulation across the rift.

**Acknowledgments**

This work is a contribution to the Natural Environment Research Council (NERC) funded RiftVolc project (NE/L013932/1, Rift volcanism: Past, present, and future). We thank all project partners for fruitful discussions and support. The comparison of the data from the reoccupied sites was undertaken by Cameron Boggon as part of a Research Experience Placement funded by NERC NE/L002558/1. RiftVolc is committed to make all compiled data publicly accessible in the National Geoscience Data Central (NGDC), UK, after the completion of the project. In the meantime, MT data can be requested from the authors. We are indebted to Dublin Institute for Advanced Studies for the instrument loan, and special thanks go to Colin Hogg for patient assistance. Administrative staff at IGGSA, Addis Ababa, were invaluable during the customs procedures. Kevin Mickus kindly provided us with the gravity data displayed in Figure 5. We thank the Editor and two reviewers for constructive comments that improved this manuscript.

## References

Agostini, A., Bonini, M., Corti, G., Sani, F., & Mazzarini, F. (2011). Fault architecture in the Main Ethiopian Rift and comparison with experimental models: Implications for rift evolution and Nubia-Somalia kinematics. *Earth and Planetary Science Letters*, *301*(3–4), 479–492.

Aizawa, K., Koyama, T., Hase, H., Uyeshima, M., Kanda, W., Utsugi, M., et al. (2014). Three-dimensional resistivity structure and magma plumbing system of the Kirishima Volcanoes as inferred from broadband magnetotelluric data. *Journal of Geophysical Research: Solid Earth*, *119*, 198–215. https://doi.org/10.1002/2013JB010682

Árnason, K., Eysteinsson, H., & Hersir, G. P. (2010). Joint 1D inversion of TEM and MT data and 3D inversion of MT data in the Hengill area, SW Iceland. *Geothermics*, *39*(1), 13–34.

Bertrand, E. A., Caldwell, T. G., Bannister, S., Soengkono, S., Bennie, S. L., Hill, G. J., & Heise, W. (2015). Using array MT data to image the crustal resistivity structure of the southeastern Taupo Volcanic Zone, New Zealand. *Journal of Volcanology and Geothermal Research*, *305*, 63–75.
Bertrand, E. A., Caldwell, T. G., Hill, G. J., Bennie, S. L., & Soengkono, S. (2013). Magnetotelluric imaging of the Ohaaki geothermal system, New Zealand: Implications for locating basement permeability. *Journal of Volcanology and Geothermal Research*, *268*, 36–45.
Beutel, E., van Wijk, J., Ebinger, C., Keir, D., & Agostini, A. (2010). Formation and stability of magmatic segments in the main ethiopian and afar rifts. *Earth and Planetary Science Letters*, *293*(3), 225–235.
Biggs, J., Bastow, I. D., Keir, D., & Lewi, E. (2011). Pulses of deformation reveal frequently recurring shallow magmatic activity beneath the Main Ethiopian Rift. *Geochemistry, Geophysics, Geosystems*, *12*(9), Q0AB10. https://doi.org/10.1029/2011GC003662
Booker, J. R. (2014). The magnetotelluric phase tensor: A critical review. *Surveys in Geophysics*, *35*(1), 7–40.
Bosworth, W. (1992). Mesozoic and early tertiary rift tectonics in East Africa. *Tectonophysics*, *209*(1–4), 115–137.
Cagniard, L. (1953). Basic Theory of the Magnetotelluric Method of Geophysical Prospecting. *Geophysics*, *18*, 605–635.
Caldwell, T. G., Bibby, H. M., & Brown, C. (2004). The magnetotelluric phase tensor. *Geophysical Journal International*, *158*(2), 457–469.
Comeau, M. J., Unsworth, M. J., Ticona, F., & Sunagua, M. (2015). Magnetotelluric images of magma distribution beneath Volcano Uturuncu, Bolivia: Implications for magma dynamics. *Geology*, *43*(3), 243–246.
Cornwell, D., Mackenzie, G., England, R., Maguire, P., Asfaw, L., & Oluma, B. (2006). Northern Main Ethiopian Rift crustal structure from new high-precision gravity data. *Geological Society, London, Special Publications*, *259*(1), 307–321.
Corti, G. (2009). Continental rift evolution: From rift initiation to incipient break-up in the Main Ethiopian Rift, East Africa. *Earth-Science Reviews*, *96*(1–2), 1–53.
Dai, L., Hu, H., Li, H., Hui, K., Jiang, J., Li, J., & Sun, W. (2015). Electrical conductivity of gabbro: The effects of temperature, pressure and oxygen fugacity. *European Journal of Mineralogy*, *27*(2), 215–224.
Daly, E., Keir, D., Ebinger, C. J., Stuart, G. W., Bastow, I. D., & Ayele, A. (2008). Crustal tomographic imaging of a transitional continental rift: The Ethiopian rift. *Geophysical Journal International*, *172*(3), 1033–1048.
Daniels, K., Bastow, I., Keir, D., Sparks, R., & Menand, T. (2014). Thermal models of dyke intrusion during development of continent–ocean transition. *Earth and Planetary Science Letters*, *385*, 145–153.
Desissa, M., Johnson, N. E., Whaler, K. A., Hautot, S., Fisseha, S., & Dawes, G. J. K. (2013). A mantle magma reservoir beneath an incipient mid-ocean ridge in Afar, Ethiopia. *Nature Geoscience*, *6*(10), 861–865.
Di Carlo, I., Rotolo, S. G., Scaillet, B., Buccheri, V., & Pichavant, M. (2010). Phase equilibrium constraints on pre-eruptive conditions of recent felsic explosive volcanism at Pantelleria Island. Italy. *Journal of Petrology*, *51*(11), 2245–2276.
Díaz, D., Heise, W., & Zamudio, F. (2015). Three-dimensional resistivity image of the magmatic system beneath Lastarria volcano and evidence for magmatic intrusion in the back arc (northern Chile). *Geophysical Research Letters*, *42*, 5212–5218. https://doi.org/10.1002/2015GL064426
Didana, Y. L., Thiel, S., & Heinson, G. (2015). Three dimensional conductivity model of the Tendaho High Enthalpy Geothermal Field, NE Ethiopia. *Journal of Volcanology and Geothermal Research*, *290*, 53–62.
Dugda, M. T., Nyblade, A. A., Julia, J., Langston, C. A., Ammon, C. J., & Simiyu, S. (2005). Crustal structure in Ethiopia and Kenya from receiver function analysis: Implications for rift development in eastern Africa. *Journal of Geophysical Research*, *110*, B01303. https://doi.org/10.1029/2004JB003065
Ebinger, C. J., & Casey, M. (2001). Continental breakup in magmatic provinces: An Ethiopian example. *Geology*, *29*(6), 527–530.
Ebinger, C. J., Keir, D., Bastow, I. D., Whaler, K., Hammond, J. O. S., Ayele, A., et al. (2017). Crustal structure of active deformation zones in Africa: Implications for global crustal processes. *Tectonics*, *36*, 3298–3332. https://doi.org/10.1002/2017TC004526
Egbert, G. D. (1997). Robust multiple-station magnetotelluric data processing. *Geophysical Journal International*, *130*(2), 475–496.
Fontijn, K., McNamara, K., Tadesse, A. Z., Pyle, D. M., Dessalegn, F., Hutchison, W., et al. (2018). Contrasting styles of post-caldera volcanism along the Main Ethiopian Rift: Implications for contemporary volcanic hazards. *Journal of Volcanology and Geothermal Research*, *356*, 90–113.
Furman, T., Bryce, J., Rooney, T., Hanan, B., Yirgu, G., & Ayalew, D. (2006). Heads and tails: 30 million years of Afar plume. In G. Yirgu, C. J. Ebinger, & P. K. H. Maguire (Eds.), *Afar volcanic province within the East African Rift System, Geological Society Special Publication, Ethiopian Geosci & Mineral Engn Assoc. International Conference on East African Rift Systems - Geodynamics, Resources and Environment* (Vol. 259, pp. 95–119). Addis Ababa, Ethipia, Jun 2004.
Gaillard, F. (2004). Laboratory measurements of electrical conductivity of hydrous and dry silicic melts under pressure. *Earth and Planetary Science Letters*, *218*(1-2), 215–228.
Gleeson, M. L. M., Stock, M. J., Pyle, D. M., Mather, T. A., Hutchison, W., Yirgu, G., & Wade, J. (2017). Constraining magma storage conditions at a restless volcano in the Main Ethiopian Rift using phase equilibria models. *Journal of Volcanology and Geothermal Research*, *337*, 44–61.
Guo, X., Zhang, L., Behrens, H., & Ni, H. (2016). Probing the status of felsic magma reservoirs: Constraints from the P-T-$H_2O$ dependences of electrical conductivity of rhyolitic melt. *Earth and Planetary Science Letters*, *433*, 54–62.
Hashin, Z., & Shtrikman, S. (1962). A variational approach to theory of effective magnetic permeability of mulitphase materials. *Journal of Applied Physics*, *33*(10), 3125–3131.
Heise, W., Caldwell, T. G., Bibby, H. M., & Bennie, S. L. (2010). Three-dimensional electrical resistivity image of magma beneath an active continental rift, Taupo Volcanic Zone, New Zealand. *Geophysical Research Letters*, *37*, L10301. https://doi.org/10.1029/2010GL043110
Hunt, J. A., Zafu, A., Mather, T. A., Pyle, D. M., & Barry, P. H. (2017). Spatially variable $CO_2$ degassing in the Main Ethiopian Rift: Implications for magma storage, volatile transport and rift-related emissions. *Geochemistry, Geophysics, Geosystems*, *18*, 3714–3737. https://doi.org/10.1002/2017GC006975
Hutchison, W., Biggs, J., Mather, A., Pyle, T., Lewi, D., Yirgu, E., et al. (2016). Causes of unrest at silicic calderas in the East African Rift: New constraints from InSAR and soil-gas chemistry at Aluto volcano, Ethiopia. *Geochemistry, Geophysics, Geosystems*, *17*, 3008–3030. https://doi.org/10.1002/2016GC006395
Hutchison, W., Mather, T. A., Pyle, D. M., Biggs, J., & Yirgu, G. (2015). Structural controls on fluid pathways in an active rift system: A case study of the Aluto volcanic complex. *Geosphere*, *11*(3), 542–562.
Hutchison, W., Pyle, D. M., Mather, T. A., Yirgu, G., Biggs, J., Cohen, B. E., et al. (2016). The eruptive history and magmatic evolution of Aluto volcano: New insights into silicic peralkaline volcanism in the Ethiopian rift. *Journal of Volcanology and Geothermal Research*, *328*, 9–33.
Johnson, N. E., Whaler, K. A., Hautot, S., Fisseha, S., Desissa, M., & Dawes, G. J. K. (2015). Magma imaged magnetotellurically beneath an active and an inactive magmatic segment in Afar, Ethiopia. In T. Wright, A. Ayele, D. Ferguson, T. Kidane, & C. Vye-Brown (Eds.), *Magmatic rifting and active volcanism* (Vol. 420, pp. 105–125). Geological Society, London, Special Publications.
Kalscheuer, T., de los Ángeles García Juanatey, M., Meqbel, N., & Pedersen, L. B. (2010). Non-linear model error and resolution properties from two-dimensional single and joint inversions of direct current resistivity and radiomagnetotelluric data. *Geophysical Journal International*, *182*(3), 1174–1188.

Kalscheuer, T., Pedersen, L. B., & Siripunvaraporn, W. (2008). Radiomagnetotelluric two-dimensional forward and inverse modelling accounting for displacement currents. *Geophysical Journal International*, *175*(2), 486–514.
Keir, D., Bastow, I. D., Corti, G., Mazzarini, F., & Rooney, T. O. (2015). The origin of along-rift variations in faulting and magmatism in the ethiopian rift. *Tectonics*, *34*, 464–477. https://doi.org/10.1002/2014TC003698
Keir, D., Stuart, G. W., Jackson, A., & Ayele, A. (2006). Local earthquake magnitude scale and seismicity rate for the Ethiopian rift. *Bulletin of the Seismological Society of America*, *96*(6), 2221–2230.
Kim, S., Nyblade, A. A., Rhie, J., Baag, C.-E., & Kang, T.-S. (2012). Crustal S-wave velocity structure of the Main Ethiopian Rift from ambient noise tomography. *Geophysical Journal International*, *191*(2), 865–878.
Kogan, L., Fisseha, S., Bendick, R., Reilinger, R., McClusky, S., King, R., & Solomon, T. (2012). Lithospheric strength and strain localization in continental extension from observations of the East African Rift. *Journal of Geophysical Research*, *117*, B03402. https://doi.org/10.1029/2011JB008516
Krumrei, T. V., Villa, I. M., Marks, M. A., & Markl, G. (2006). A 40Ar/39Ar and U/Pb isotopic study of the Ilimaussaq complex, South Greenland: Implications for the 40K decay constant and for the duration of magmatic activity in a peralkaline complex. *Chemical Geology*, *227*(3), 258–273.
Lewi, E., Keir, D., Birhanu, Y., Blundy, J., Stuart, G., Wright, T., & Calais, E. (2016). Use of a high-precision gravity survey to understand the formation of oceanic crust and the role of melt at the southern Red Sea rift in Afar, Ethiopia. In T. J. Wright, A. Ayele, D. J. Ferguson, T. Kidane, & C. VyeBrown (Eds.), *Magmatic rifting and active volcanism* (Vol. 420, pp. 165–180). Geological Society, London, Special Publications.
Mackenzie, G. D., Thybo, H., & Maguire, P. K. H. (2005). Crustal velocity structure across the Main Ethiopian Rift: Results from two-dimensional wide-angle seismic modelling. *Geophysical Journal International*, *162*(3), 994–1006.
Mahatsente, R., Jentzsch, G., & Jahr, T. (1999). Crustal structure of the Main Ethiopian Rift from gravity data: 3-dimensional modeling. *Tectonophysics*, *313*(4), 363–382.
Mazzarini, F., & Isola, I. (2010). Monogenetic vent self-similar clustering in extending continental crust: Examples from the East African Rift System. *Geosphere*, *6*(5), 567–582.
Mazzarini, F., Le Corvec, N., Isola, I., & Favalli, M. (2016). Volcanic field elongation, vent distribution, and tectonic evolution of a continental rift: The Main Ethiopian Rift example. *Geosphere*, *12*(3), 706–720.
Mazzarini, F., Rooney, T. O., & Isola, I. (2013). The intimate relationship between strain and magmatism: A numerical treatment of clustered monogenetic fields in the Main Ethiopian Rift. *Tectonics*, *32*, 49–64. https://doi.org/10.1029/2012TC003146
McBirney, A. (1996). The Skaergaard intrusion. In R. G. Cawthorn (Ed.), *Layered intrusions* (Vol. 15, pp. 147–180). Elsevier, Developments in Petrology.
Mickus, K., Tadesse, K., Keller, G. R., & Oluma, B. (2007). Gravity analysis of the main Ethiopian rift. *Journal of African Earth Sciences*, *48*(2–3), 59–69.
Miensopust, M. P., Jones, A. G., Hersir, G. P., & Vilhjálmsson, A. M. (2014). The Eyjafjallajökull volcanic system, Iceland: Insights from electromagnetic measurements. *Geophysical Journal International*, *199*, 1187–1204.
Mohr, P. (1967). Major volcano-tectonic lineament in the Ethiopian Rift System. *Nature*, *213*(5077), 664–665.
Mwarikani, R. (2015). Integrated geophysical model for Suswa geothermal prospect using resistivity, seismics and gravity survey data in Kenya. In *Proceedings World Geothermal Congress, Melbourne, Australia* (pp. 6). Melbourne, Australia, 19-25 April 2015.
Peccerillo, A., Barberio, M., Yirgu, G., Ayalew, D., Barbieri, M., & Wu, T. (2003). Relationships between mafic and peralkaline silicic magmatism in continental rift settings: A petrological, geochemical and isotopic study of the Gedemsa volcano, central Ethiopian rift. *Journal of Petrology*, *44*(11), 2003–2032.
Pedersen, L. B., & Engels, M. (2005). Routine 2D inversion of magnetotelluric data using the determinant of the impedance tensor. *Geophysics*, *70*(2), G33–G41.
Pommier, A. (2014). Interpretation of magnetotelluric results using laboratory measurements. *Surveys in Geophysics*, *35*(1), 41–84.
Pommier, A., Gaillard, F., Malki, M., & Pichavant, M. (2010). Methodological re-evaluation of the electrical conductivity of silicate melts. *American Mineralogist*, *95*(2-3), 284–291.
Pommier, A., & Le-Trong, E. (2011). "SIGMELTS": A web portal for electrical conductivity calculations in geosciences. *Computers & Geosciences*, *37*(9), 1450–1459.
Pous, J., Poyatos Martínez, D., Heise, W., Santos, F. M., Galindo-Zaldívar, J., Ibarra, P., et al. (2011). Constraints on the crustal structure of the internal Variscan Belt in SW Europe: A magnetotelluric transect along the eastern part of Central Iberian Zone, Iberian Massif. *Journal of Geophysical Research*, *116*, B02103. https://doi.org/10.1029/2010JB007538
Roberts, J., & Tyburczy, J. (1999). Partial-melt electrical conductivity: Influence of melt composition. *Journal of Geophysical Research*, *104*(B4), 7055–7065.
Rooney, T. O. (2010). Geochemical evidence of lithospheric thinning in the southern Main Ethiopian Rift. *Lithos*, *117*(1–4), 33–48.
Rooney, T., Furman, T., Bastow, I., Ayalew, D., & Yirgu, G. (2007). Lithospheric modification during crustal extension in the Main Ethiopian Rift. *Journal of Geophysical Research*, *112*, B10201. https://doi.org/10.1029/2006JB004916
Rooney, T. O., Furman, T., Yirgu, G., & Ayalew, D. (2005). Structure of the Ethiopian lithosphere: Xenolith evidence in the Main Ethiopian Rift. *Geochimica et Cosmochimica Acta*, *69*(15), 3889–3910.
Rosenkjaer, G. K., Gasperikova, E., Newman, G. A., Arnason, K., & Lindsey, N. J. (2015). Comparison of 3D MT inversions for geothermal exploration: Case studies for Krafla and Hengill geothermal systems in Iceland. *Geothermics*, *57*, 258–274.
Saibi, H., Aboud, E., & Ehara, S. (2012). Analysis and interpretation of gravity data from the Aluto-Langano geothermal field of Ethiopia. *Acta Geophysica*, *60*(2), 318–336.
Samrock, F., Kuvshinov, A., Bakker, J., Jackson, A., & Fisseha, S. (2015). 3-D analysis and interpretation of magnetotelluric data from the Aluto-Langano geothermal field, Ethiopia. *Geophysical Journal International*, *202*(3), 1923–1948.
Schmeling, H. (1986). Numerical models on the influence of partial melt on elastic, anelastic and electrical properties of rocks. 2: Electrical conductivity. *Physics of the Earth and Planetary Interiors*, *43*(2), 123–136.
Selway, K. (2015). Negligible effect of hydrogen content on plate strength in East Africa. *Nature Geoscience*, *8*(7), 543–546.
Sigmundsson, F., Hreinsdóttir, S., Hooper, A., Árnadóttir, T., Pedersen, R., Roberts, M. J., et al. (2010). Intrusion triggering of the 2010 Eyjafjallajökull explosive eruption. *Nature*, *468*(7322), 426–430.
Siripunvaraporn, W., & Egbert, G. (2000). An efficient data-subspace inversion method for 2-D magnetotelluric data. *Geophysics*, *65*(3), 791–803.
Smirnov, M. Y. (2003). Magnetotelluric data processing with a robust statistical procedure having a high breakdown point. *Geophysical Journal International*, *152*(1), 1–7.

Stuart, G. W., Bastow, I. D., & Ebinger, C. J. (2006). Crustal structure of the northern Main Ethiopian Rift from receiver function studies. In G. Yirgu, C. J. Ebinger, & P. K. H. Maguire (Eds.), *The Afar volcanic province within the East African Rift System, Geological Society Special Publication, Ethiopian Geosci & Mineral Engn Assoc. International Conference on East African Rift Systems - Geodynamics, Resources and Environment* (Vol. 259, pp. 253–267). Addis Ababa, Ethipia, Jun 2004.

Teklemariam, M., Battaglia, S., Gianelli, G., & Ruggieri, G. (1996). Hydrothermal alteration in the Aluto-Langano geothermal field, Ethiopia. *Geothermics*, *25*(6), 679–702.

Tikhonov, A. N. (1950). On determination of electric characteristics of deep layers of the Earth's crust. *Doklady*, *73*, 295–297.

Wameyo, P. (2005). Magnetotelluric and transient electromagnetic methods in geothermal prospecting, with examples from Menegai, Kenya (Report 21). UNU-GTP, Iceland: Geothermal Training in Iceland 2005.

Whaler, K. A., & Hautot, S. (2006). The electrical resistivity structure of the crust beneath the northern Main Ethiopian Rift. In G. Yirgu, C. J. Ebinger, & P. K. H. Maguire (Eds.), *The Afar volcanic province within the East African Rift System, Geological Society Special Publication, Ethiopian Geosci & Mineral Engn Assoc. International Conference on East African Rift Systems – Geodynamics, Resources and Environment* (Vol. 259, pp. 293–305). Addis Ababa, Ethipia, Jun 2004.

Wilks, M., Ayele, A., Kendall, J. M., & Wookey, J. (2017). The 24th January 2016 Hawassa earthquake: Implications for seismic hazard in the Main Ethiopian Rift. *Journal of African Earth Sciences*, *125*, 118–125.

Wilks, M., Kendall, J.-M., Nowacki, A., Biggs, J., Wookey, J., Birhanu, Y., et al. (2017). Seismicity associated with magmatism, faulting and hydrothermal circulation at Aluto Volcano, Main Ethiopian Rift. *Journal of Volcanology and Geothermal Research*, *340*, 52–67.

Woldegabriel, G., Aronson, J. L., & Walter, R. C. (1990). Geology, geochronology, and rift basin development in the central sector of the main Ethiopia rift. *GSA Bulletin*, *102*(4), 439–458.

Zhang, P., Roberts, R. G., & Pedersen, L. B. (1987). Magnetotelluric strike rules. *Geophysics*, *52*(3), 267–278.